*materials*

MDPI

*Article*

# Phase Evolution and Mullite Formation in Refractory Aluminosilicate Ceramics Based on Natural and Synthetic Raw Materials

**Lazzat Shansharova [1], Rimma Niyazbekova [1,2,*], Tynyshkul Amreyeva [1], Dzhumakhon Sharifov [3], Mira Serekpayeva [1] and Michał Bembenek [4,*]**

[1] Department of Standardization, Metrology and Certification, Technical Faculty, Saken Seifullin Kazakh Agrotechnical University", 62 Zhenis Ave., Astana 010011, Kazakhstan; l.sarsenbayevna@gmail.com (L.S.); amreeva_tm@mail.ru (T.A.); mika82.0242@gmail.com (M.S.)
[2] "Kazakhstan Institute of Standardization and Metrology" Republican State Enterprise, 11 Mangilik El Ave., Astana 010000, Kazakhstan
[3] Department of "Radio engineering, electronics and telecommunications", Institute of Physics and Technology , L.N. Gumilyov Eurasian National University, Astana 010008, Kazakhstan; shjumm@mail.ru
[4] Faculty of Mechanical Engineering and Robotics, AGH University of Krakow, A. Mickiewicza 30, 30-059 Krakow, Poland
* Correspondence: niazbekovarimma@gmail.com (R.N.); bembenek@agh.edu.pl (M.B.)

## Highlights

- Fly ash was successfully used as a secondary aluminosilicate raw material for mullite-containing ceramics.
- KER-1 fired at 1300 °C exhibited the highest quantified mullite content of 42.02 wt%.
- Increasing the firing temperature to 1450 °C promoted microstructural densification but did not universally increase mullite content.
- XRD/WPPF, SEM, and FTIR revealed the relationship between phase evolution and microstructural development.

## Abstract

This study investigates the potential of using fly ash from thermal power plants as an aluminosilicate component in the production of kaolin-based refractory ceramics. Kaolin, fly ash, and chalk were used as starting materials, and experimental compositions containing 30–60 wt% fly ash were fired at 1200, 1300, and 1450 °C. X-ray diffraction with whole powder pattern fitting (WPPF) was used to determine phase composition and phase transformations, while scanning electron microscopy (SEM) and Fourier-transform infrared (FTIR) spectroscopy were employed to characterize microstructural and structural changes. The results demonstrate that the phase composition of the fired ceramics depends on both the initial composition and firing temperature. Quartz, mullite, and cristobalite were identified as the main crystalline phases in the fired ceramics. The detected mullite may partly originate from the pre-existing mullite phase in the fly ash, which remained present after high-temperature firing. The KER-1 composition fired at 1300 °C exhibited the highest relative proportion of mullite among the quantified crystalline phases (42.02 wt%), together with quartz (29.19 wt%) and β-cristobalite (27.20 wt%). At 1450 °C, the relative mullite proportion decreased to 21.02 wt%, while quartz increased to 73.71 wt%. These WPPF values represent normalized fractions of crystalline phases rather than absolute contents in the bulk samples. SEM observations indicated more pronounced sintering and improved intergranular contacts at 1450 °C, while FTIR analysis revealed

Academic Editor: Vincenzo M. Sglavo

Received: 19 October 2026
Revised: 25 November 2026
Accepted: 26 November 2026
Published: 29 November 2026

**Copyright:** © 2026 by the authors. Licensee MDPI, Basel, Switzerland. This article is an open access article distributed under the terms and conditions of the Creative Commons Attribution (CC BY) license.

changes in the aluminosilicate structure, dehydroxylation of kaolin, and decomposition of carbonate-containing phases. The results demonstrate that the crystalline phase composition depends on both raw material composition and firing temperature. KER-1 fired at 1300 °C exhibited the highest relative mullite proportion, whereas firing at 1450 °C promoted more pronounced sintering.

**Keywords:** refractory materials; fly ash; aluminosilicate raw materials; high-temperature firing

## 1. Introduction

Fly ash, which is produced during coal combustion at thermal power plants, is considered one of the most significant secondary mineral resources in the energy industry. Its production in large quantities and variations in chemical and mineralogical composition give rise to both environmental problems associated with waste accumulation and the potential for its use as a raw material for producing new materials. Unlike traditional natural aluminosilicates, the composition of fly ash varies significantly depending on the type of coal, the mineral composition of the fuel, combustion conditions, and ash capture technology. As a result, the content of $SiO_2$, $Al_2O_3$, $Fe_2O_3$, CaO, and other components, as well as the ratio of crystalline to amorphous phases, can vary significantly [1–3]. It is precisely this variability that determines both the potential applications of fly ash and the need to adapt technological approaches to its specific composition.

Fly ash is most widely used in the production of cement and concrete, construction composites, geopolymer materials, road bases, and for soil stabilization [4–7]. A significant body of research is also devoted to the production of ceramic materials and products using fly ash as a secondary raw material. It has been shown that the presence of an aluminosilicate glass phase and crystalline components makes fly ash a promising starting material for the formation of ceramic phases during heat treatment [8–10]. At the same time, most of the published studies focus on the use of ash as a filler, a pozzolanic component, or a source of $SiO_2$ and $Al_2O_3$. In contrast, its targeted use for forming a high-temperature mullite-containing structure has been studied much less systematically.

Of particular interest in this context is the production of aluminosilicate refractories. Materials of the $Al_2O_3$–$SiO_2$ system are widely used in high-temperature processes due to their combination of refractoriness, mechanical strength, chemical resistance, and thermal stability [11–13]. Among the phases that determine the performance properties of such materials, mullite ($3Al_2O_3{\cdot}2SiO_2$) is of particular importance, as it is characterized by high thermal stability, a low coefficient of thermal expansion, and stability at high temperatures [14–16]. Therefore, controlling the conditions for mullite formation is one of the key areas in the development of aluminosilicate refractory ceramics.

The traditional production of mullite-containing refractories is based primarily on the use of kaolin, high-alumina raw materials, bauxite, and other natural materials with adjustable $Al_2O_3$ and $SiO_2$ contents [17–19]. However, the cost and limited availability of high-quality natural raw materials are driving the search for secondary aluminosilicate components. In this regard, fly ash is of interest as a potential source of $SiO_2$–$Al_2O_3$ components, capable of partially replacing natural raw materials while simultaneously increasing the extent to which industrial waste is incorporated into the production of functional materials [20–22].

Research in recent years has confirmed the fundamental possibility of producing ceramic and refractory materials using fly ash. It has been shown that at elevated temperatures, the aluminosilicate components contained in the ash participate in processes of

solid-state interaction, liquid-phase formation, sintering, and the formation of new crystalline phases [23–25]. Some studies report the formation of mullite during the thermal treatment of fly ash and its mixtures with kaolin or other aluminosilicate materials [26]. However, the results of these studies depend significantly on the origin of the ash, its chemical composition, the ratio of the starting components, and the temperature-time profile of the firing process. Therefore, it is difficult to directly apply the established patterns to different types of ash.

The existing literature allows us to identify several unresolved issues. First, the influence of the specific chemical composition of fly ash on the direction of phase formation during co-firing with kaolin remains insufficiently systematized. Second, most studies focus primarily on the final mechanical or performance characteristics of the materials. At the same time, the relationship between the composition of the starting mixture, firing temperature, mullite phase formation, and microstructural changes is addressed only in a piecemeal fashion. Third, the composition of ceramic mixtures is often selected empirically, without first determining the composition's position in the multicomponent $Al_2O_3$–$SiO_2$–CaO system. As a result, the question of what degree of kaolin substitution with fly ash provides the most favorable conditions for the formation of a mullite-containing structure at various firing temperatures remains insufficiently studied.

Thus, the existing research gap lies not in the absence of studies on the use of fly ash in ceramics per se, but in the insufficient understanding of the patterns of phase formation in the "kaolin–fly ash" system, taking into account its chemical composition, CaO content, and firing temperature, as well as the lack of a unified approach to justifying the composition of such mixtures based on the $Al_2O_3$–$SiO_2$–CaO phase diagram. Filling this gap is important for the transition from a general approach of "ash utilization in ceramics" to the controlled formation of a specified phase composition and microstructure of refractory materials.

In this study, to address this gap, the phase diagram of the $Al_2O_3$–$SiO_2$–CaO system was used to preliminarily determine the composition of experimental mixtures with varying degrees of kaolin substitution by fly ash. The thermodynamic description of the CaO–$Al_2O_3$–$SiO_2$ system has been extensively developed through critical assessments of experimental phase-equilibrium data and CALPHAD-based modelling. Eriksson and Pelton [27] performed a comprehensive evaluation and optimization of the thermodynamic properties and phase diagrams of the constituent binary systems and the ternary CaO–$Al_2O_3$–$SiO_2$ system. Subsequently, Eriksson et al. [28] carried out a thermodynamic assessment of this ternary system using the CALPHAD approach, providing calculated phase diagrams, isothermal sections, and a projection of the liquidus surface. Experimental investigations by Haccuria et al. [29] further contributed to the validation of phase-equilibrium data through the determination of liquidus isotherms in selected compositional regions. More recently, Abdul [30] presented an optimized ternary liquidus projection of the CaO–$Al_2O_3$–$SiO_2$ system, with calculated isotherms at 100 °C intervals, providing an additional reference for interpreting phase relationships at elevated temperatures.

These thermodynamic and experimental assessments provide an important basis for evaluating the compositional relationships and potential phase formation in aluminosilicate materials containing calcium oxide. In the present study, the ternary phase diagram was therefore used as a preliminary compositional selection tool for designing kaolin–fly ash mixtures with controlled CaO content.

Chalk was used as a corrective additive to regulate the CaO content and the composition positions within the ternary system. The resulting compositions were studied after firing at various temperatures to establish the relationship between fly ash content, heat treatment temperature, phase composition, and microstructure of the material.

The objective of this study is to identify the patterns governing the formation of mullite-containing refractory ceramics when kaolin is partially replaced by fly ash, based on a preliminary compositional analysis of the $Al_2O_3$–$SiO_2$–CaO system.

To achieve this objective, the following tasks were addressed:

- To determine the chemical and mineralogical composition of kaolin and fly ash;
- To justify the composition of experimental ceramic mixtures with varying degrees of kaolin replacement by fly ash using the $Al_2O_3$–$SiO_2$–CaO phase diagram;
- To determine the effect of fly ash content and firing temperature on the phase composition of the materials;
- To investigate changes in the microstructure of the resulting ceramics using X-ray phase analysis and scanning electron microscopy;
- To determine the range of fly ash content and firing temperature that ensures the formation of a mullite-containing structure, which is promising for the production of refractory ceramic materials.

The scientific novelty of this study lies in the experimental investigation of mullite-containing phase formation in a specific kaolin–fly ash–chalk system using fly ash from Ekibastuz State District Power Plant No. 1 (Kazakhstan). The study examines the influence of the initial oxide composition, fly ash content, and firing temperature on the development of crystalline phases, with particular emphasis on mullite formation. Quantitative phase analysis using the Whole Powder Pattern Fitting (WPPF) method was applied to characterize the crystalline phase composition of the fired materials. The research therefore provides experimental data on phase development in a specific aluminosilicate raw material system incorporating industrial fly ash.

## 2. Materials and Methods

### *2.1. Raw Materials Characterization*

Fly ash, a kaolin-containing refractory material, and chalk were used in this study. The fly ash was obtained from the Ekibastuz State District Power Plant No. 1 (Pavlodar Region, Kazakhstan). Kaolin from the Alekseevskoye deposit, supplied by Qazaq Kaolin LLP (Zerenda District, Akmola Region, Kazakhstan), was used as the aluminosilicate component. Chalk was used as a calcium-containing mineral additive to ensure the supply of CaO during the thermal decomposition of calcium carbonate.

The chemical composition of the raw materials (kaolin, fly ash, and chalk) was determined using a PANalytical Epsilon 1 X-ray fluorescence (XRF) spectrometer (PANalytical B.V., Almelo, The Netherlands). The concentrations of the major oxides ($SiO_2$, $Al_2O_3$, $Fe_2O_3$, CaO, $TiO_2$, MgO, and $K_2O$) were determined and expressed in weight percentages (wt%). The obtained results were used to characterize the chemical composition of the starting materials and assess their suitability for the production of mullite-containing refractory materials.

### *2.2. Selection of Experimental Formulations Based on the $Al_2O_3$–$SiO_2$–CaO Diagram*

The experimental compositions were selected using a three-component phase diagram of the $Al_2O_3$–$SiO_2$–CaO system (Figure 1). The diagram was used to determine the position of the calculated compositions relative to the stability regions of the aluminosilicate phases and to select compositions that were potentially favorable for the formation of a mullite-containing ceramic structure.

In the first stage, the $SiO_2$, $Al_2O_3$, and CaO contents in the starting components were determined based on XRF results. In the second stage, the contents of these oxides in each experimental charge were calculated, taking into account the mass fractions of fly ash,

kaolin, and chalk. The obtained values of $SiO_2$, $Al_2O_3$, and CaO were normalized to 100% and plotted on a three-component $Al_2O_3$–$SiO_2$–CaO diagram.

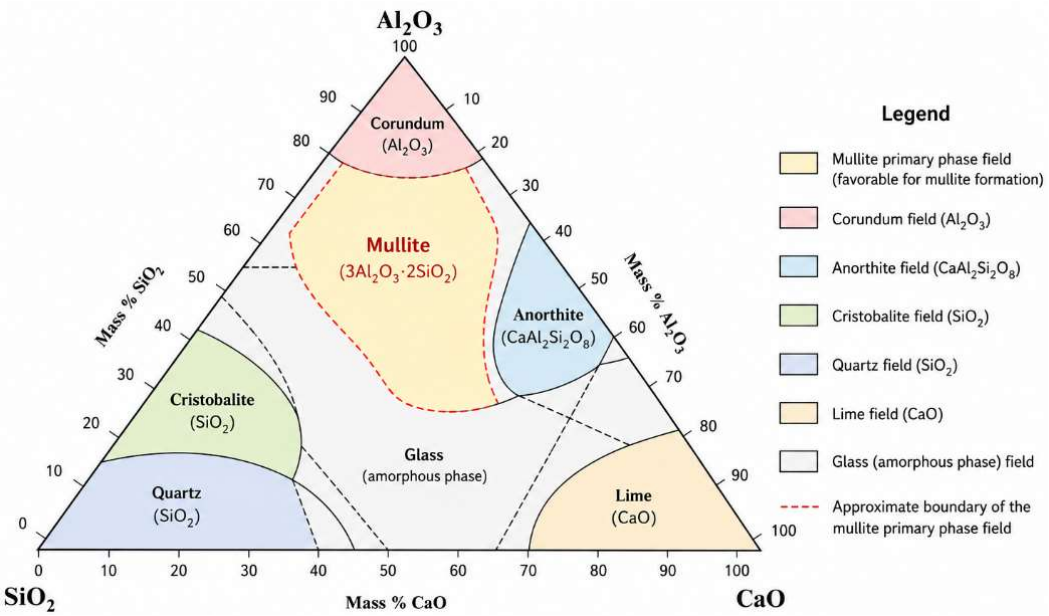



**Figure 1.** Ternary phase diagram of the $Al_2O_3$–$SiO_2$–CaO system with the mullite primary phase field highlighted (adapted from [31]).

The experimental compositions KER-1, KER-2, and KER-3 were selected using the $Al_2O_3$–$SiO_2$–CaO ternary phase diagram based on the chemical composition of the starting components, as determined by XRF. The $SiO_2$, $Al_2O_3$, and CaO contents in each batch were calculated taking into account the mass fractions of kaolin, fly ash, and chalk, and then normalized to 100%. To determine the coordinates of the experimental compositions on the $Al_2O_3$–$SiO_2$–CaO ternary diagram, the content of each of the three oxides was normalized relative to their total content using the following formula (1):

$$Xi = \frac{Ci}{C\mathrm{SiO2} + C\mathrm{Al2O3} + C\mathrm{CaO}} \times 100 \quad (1)$$

where $Xi$ is the normalized content of the corresponding $i$ oxide in the $Al_2O_3$–$SiO_2$–CaO ternary system, wt%; $Ci$ is the calculated content of the corresponding oxide in the feedstock, wt%; $C_{SiO2} + C_{Al2O3} + C_{CaO}$ are the calculated contents of $SiO_2$, $Al_2O_3$, and CaO, respectively.

The calculated composition coordinates were as follows: KER-1—59.89% $SiO_2$, 35.93% $Al_2O_3$, and 4.17% CaO; KER-2—55.53% $SiO_2$, 41.73% $Al_2O_3$, and 2.74% CaO; KER-3—56.98% $SiO_2$, 39.80% $Al_2O_3$, and 3.21% CaO. Experimental points were selected to form a sequential series of compositions with an increase in fly ash content from 30 to 60 wt% and a corresponding change in the $SiO_2/Al_2O_3$ ratio in the system. The position of the selected compositions was evaluated relative to the region where mullite-containing phases form.

The main variable parameter was the fly ash content. KER-1 contained 60 wt% fly ash, KER-2 contained 30 wt% fly ash, and KER-3 contained 40 wt% fly ash, while chalk was fixed at 1 wt% and the kaolin content was adjusted accordingly to maintain a total batch mass of 100 wt%.

This approach made it possible to investigate the effect of changes in the ratio of fly ash to kaolin-containing raw materials—and the associated change in the $SiO_2/Al_2O_3$ ratio—on phase formation and microstructure development at various firing temperatures.

The control composition KER-0 was also used for a comparative assessment of phase and structural changes.

### *2.3. Preparation of Experimental Formulations and Samples*

Based on this approach, three experimental compositions (KER-1, KER-2, and KER-3) were selected, containing 30, 40, and 60 wt% fly ash, respectively, with the kaolin content adjusted accordingly and the CaO contribution controlled by maintaining a constant chalk addition of 1 wt%. Their positions are indicated in the $Al_2O_3$–$SiO_2$–CaO diagram in Figure 1. This selection enabled the investigation of phase development across different degrees of kaolin substitution by fly ash while maintaining a comparable calcium oxide contribution.

The starting materials were dried at 105 ± 5 °C until a constant mass was reached; the drying time was at least 24 h. After drying, the components were weighed separately using laboratory scales with a resolution of 0.01 g.

The experimental compositions were prepared based on the dry mass of the components. The nominal composition of the tested mixtures is presented in Table 1.

**Table 1.** Composition of experimental ceramic mixtures, wt%.

| Sample | Kaolin | Fly Ash | Chalk | Total |
|---|---|---|---|---|
| KER-0 | 100 | - | - | 100 |
| KER-1 | 39 | 60 | 1 | 100 |
| KER-2 | 69 | 30 | 1 | 100 |
| KER-3 | 59 | 40 | 1 | 100 |

The control composition, KER-0, consisted of the raw kaolin without the addition of fly ash or chalk. Thus, KER-0 characterized the phase transformations and microstructural changes in the raw aluminosilicate material at the same heat treatment temperatures. Kaolin and fly ash were initially mixed in the dry state for 10 min to obtain a homogeneous mixture. Then, 1 mass % of chalk was added, and the mixture was stirred for an additional 5 min.

No water or additional binding agents were used in the preparation of the mixture. The total mass of each prepared mixture was 100 g.

After mixing, the prepared mixture was placed directly into fireclay crucibles. The material was fired as a powdered mixture in the fireclay crucibles. The mixtures were not subjected to joint mechanochemical activation or uniaxial pressing before firing. Therefore, the experiments were conducted using dry-mixed powder batches without preliminary compaction.

### *2.4. Heat Treatment*

Heat treatment was performed in a Nabertherm high-temperature electric chamber furnace with a maximum operating temperature of 1600 °C and programmable temperature control. The samples were placed in fireclay crucibles and fired at temperatures of 1200, 1300, and 1450 °C. The experimental compositions were prepared and subjected to firing under the conditions specified in Table 2. The manuscript reports the results obtained from the prepared samples. Independent batch preparations and replicate firing runs were not conducted. The analytical measurements were performed on the obtained samples, and the reported results correspond to the measurements carried out for each investigated condition.

**Table 2.** Heat treatment conditions for experimental compositions.

| Sample | Temperature, °C | Heating Time, h | Exposure Time, min | Cooling |
|---|---|---|---|---|
| KER-0 | 1200 | 4 | 60 | in the furnace |
| KER-0 | 1300 | 4 | 60 | in the furnace |
| KER-0 | 1450 | 4 | 60 | in the furnace |
| KER-1 | 1200 | 4 | 60 | in the furnace |
| KER-1 | 1300 | 4 | 60 | in the furnace |
| KER-1 | 1450 | 4 | 60 | in the furnace |
| KER-2 | 1200 | 4 | 60 | in the furnace |
| KER-2 | 1300 | 4 | 60 | in the furnace |
| KER-2 | 1450 | 4 | 60 | in the furnace |
| KER-3 | 1200 | 4 | 60 | in the furnace |
| KER-3 | 1300 | 4 | 60 | in the furnace |
| KER-3 | 1450 | 4 | 60 | in the furnace |

The samples were heated from room temperature to each specified temperature (1200, 1300, or 1450 °C) over a period of 4 h. Once the set temperature was reached, the samples were held at that temperature for 60 min. The furnace was then turned off, and the samples were allowed to cool inside the furnace to room temperature.

After the isothermal holding period was complete, the furnace was turned off, and the samples were cooled directly in the furnace chamber to room temperature. Forced cooling was not used.

Heat treatment of the experimental samples in a Nabertherm high-temperature electric furnace (Nabertherm GmbH, Lilienthal, Germany). Placing the specimens in fireclay crucibles, heating them to the specified temperatures of 1200, 1300, and 1450 °C, holding them at the maximum temperature for 60 min, and subsequently cooling the specimens in the furnace to room temperature.

Although all compositions were fired at 1200, 1300, and 1450 °C, detailed characterization was focused on the conditions most informative for evaluating phase evolution and microstructural development.

### *2.5. X-Ray Diffraction Analysis and Quantitative Phase Analysis*

X-ray diffraction (XRD) analysis was performed to identify the crystalline phases formed in the ceramic samples after firing at 1300 and 1450 °C. The samples were ground to a fine powder prior to analysis to ensure representative phase characterization and minimize the influence of particle orientation.

XRD measurements were carried out using a Rigaku SmartLab diffractometer (Rigaku, Tokyo, Japan) with Cu K$\alpha$ radiation.

Phase identification was performed using the Powder Diffraction File (PDF-2) database, Release 2024 (International Centre for Diffraction Data, ICDD)

. The experimental diffraction patterns were analyzed using the Powder XRD Plugin implemented in Rigaku SmartLab software (version 4.4.0.0; Rigaku Corporation, Japan). Quantitative phase analysis was performed using the Whole Powder Pattern Fitting (WPPF) method based on the Fundamental Parameters (FP) approach. The X-ray source was a CuKa (1.54059) X-ray tube (Rigaku Corporation, Akishima, Tokyo, Japan). The tube current and voltage were set to 50 mA and 40 kV, respectively. A one-dimensional detector (D/teX Ultra, Rigaku) (Akishima, Tokyo, Japan) with a Kß filter was used. Measurements were performed using the step-scanning method under the following conditions: measurement angle range 2θ = 5–90°, step width (δ2θ) = 0.1°, and scanning speed = 2 deg/min.

In the WPPF analysis, the entire experimental diffraction pattern was fitted rather than individual diffraction peaks. The calculated pattern was obtained by refining the contributions of the identified crystalline phases to the experimental profile. Phase identification was based on the positions and relative intensities of characteristic reflections, while quantitative phase fractions were determined from the refined whole-pattern profile. The crystalline phases included in the refinement were selected according to the experimentally identified phase assemblage and the corresponding entries in the PDF-2 database.

The WPPF refinement was performed using the instrumental profile description based on the Fundamental Parameters approach implemented in the Rigaku SmartLab software. The refinement procedure included adjustment of the profile and phase-related parameters to achieve the best agreement between the calculated and experimental diffraction patterns. The quantitative phase contents are reported as weight percentages of the crystalline phases included in the refinement.

The obtained quantitative phase compositions were subsequently compared with the SEM observations and FTIR results to provide a comprehensive interpretation of phase formation, sintering, and structural development during firing.

### *2.6. Fourier Transform Infrared Spectroscopy*

Fourier-transform infrared (FTIR) spectroscopy was used to study changes in the chemical and structural properties of the aluminosilicate matrix in the as-received and calcined materials.

FTIR spectra were acquired using an InfraLUM FT-08 spectrometer (Lumex Instruments, Saint Petersburg, Russia) equipped with an attenuated total reflectance (ATR) accessory. Measurements were performed over the spectral range of 400–4000 $cm^{-1}$.

### *2.7. Scanning Electron Microscopy*

The microstructure of the sintered samples was examined using scanning electron microscopy (SEM) on a TESCAN VEGA 3 scanning electron microscope (TESCAN GROUP, a.s., Brno, Czech Republic). Prior to examination, the sintered samples were dried, after which the surface was prepared by mechanically fracturing the sample to obtain a fresh fracture surface. The prepared fragments were mounted on a specimen stage for SEM analysis.

The analysis was conducted under high vacuum at an accelerating voltage of 5 kV. SEM images were acquired at magnifications of 667×, 800×, 1330×, and 4000×.

## 3. Results

### *3.1. Characteristics of Raw Materials*

The temperature range of 1200–1450 °C was chosen to study the successive stages of thermal transformations in aluminosilicate raw materials, including the dehydration and structural rearrangement of clay minerals, solid-state reactions, sintering processes, and the formation of mullite-containing phases.

The chemical compositions of the starting materials determined by X-ray fluorescence analysis are presented in Table 3. Kaolin contains 43.06 wt% $SiO_2$ and 39.97 wt% $Al_2O_3$, confirming its aluminosilicate character and its suitability as the main Al- and Si-containing component for mullite formation.

Fly ash contains 54.8 wt% $SiO_2$ and 23.7 wt% $Al_2O_3$, giving a combined $SiO_2$ + $Al_2O_3$ content of 78.5 wt%. In addition, $Fe_2O_3$, CaO, and $TiO_2$ are present. The high proportion of aluminosilicate components indicates that the fly ash can act as a secondary aluminosilicate raw material. In contrast, the minor oxide components may influence sintering, diffusion, and phase formation.

The chalk is characterized predominantly by CaO on a compositional basis (55.2 wt%), with only minor amounts of $SiO_2$, $Al_2O_3$, $Fe_2O_3$, and MgO. During firing, the calcium carbonate component decomposes, and the resulting calcium-containing phase can participate in reactions with the aluminosilicate components.

Thus, the starting materials provide the $SiO_2$- and $Al_2O_3$-containing components required for the formation of mullite and other high-temperature aluminosilicate phases. At the same time, the substantial silica content of the fly ash and kaolin is consistent with the predominance of quartz-containing phases observed in several of the fired compositions. The chemical compositions of the starting materials therefore provide an important basis for interpreting the differences in phase composition among KER-1, KER-2, and KER-3.

**Table 3.** Chemical composition of raw materials (wt%).

| Material | $SiO_2$ | $Al_2O_3$ | $Fe_2O_3$ | CaO | $TiO_2$ | MgO | $K_2O$ |
|---|---|---|---|---|---|---|---|
| Kaolin | 43.06 | 39.97 | 0.91 | 0.54 | 0.53 | 0.51 | 0.32 |
| Fly ash | 54.8 | 23.7 | 8.6 | 4.5 | 2.1 | 0.3 | |
| Chalk | 1.4 | 0.4 | 0.18 | 55.2 | – | 0.3 | |

In terms of its content of coloring oxides, kaolin is classified as a clay raw material with a low content of coloring oxides. In terms of its aluminum oxide content, kaolin is classified as a basic raw material. The results of X-ray fluorescence analysis showed that the fly ash is characterized by a high content of silicon and aluminum oxides, the combined proportion of which exceeds 78 wt%. This allows it to be considered a promising secondary aluminosilicate raw material for the production of mullite-containing refractory materials. The high content of $SiO_2$ and $Al_2O_3$ provides the necessary raw material base for high-temperature solid-phase reactions to occur and for the formation of the mullite phase during firing.

Along with the main oxides, the fly ash composition includes $Fe_2O_3$, CaO, $TiO_2$, and a negligible amount of other components. These oxides can influence sintering processes, the kinetics of phase formation, and the development of the material's microstructure. The presence of a small amount of CaO promotes the formation of a liquid phase during high-temperature processing, which intensifies the processes of diffusion and densification of the ceramic matrix. Chalk is characterized by a high calcium oxide content (approximately 55–56% on a CaO basis) and negligible amounts of $SiO_2$, $Al_2O_3$, $Fe_2O_3$, and MgO impurities. During the thermal decomposition of $CaCO_3$, CaO is formed, which is capable of interacting with the aluminosilicate matrix, thereby influencing the sintering and phase-formation processes. Thus, the chemical composition of the starting components provides the necessary conditions for high-temperature phase transformations and the formation of a mullite-containing ceramic structure. The high content of the aluminosilicate component, combined with the presence of a reactive amorphous glass phase, makes fly ash an effective component for the synthesis of mullite ceramics and contributes to the rational use of industrial waste from the energy sector.

It has been established that kaolin is characterized by a high total content of silicon and aluminum oxides, which confirms that it belongs to the category of high-alumosilicate clay raw materials widely used in the production of ceramic and refractory materials. The high content of $Al_2O_3$ and $SiO_2$ provides favorable conditions for the formation of the mullite phase during high-temperature firing.

Fly ash contains more than 78% by mass of $SiO_2$ and $Al_2O_3$ oxides, which classifies it as a low-calcium aluminosilicate ash (Class F). Due to its high content of reactive aluminosilicate components, fly ash can be considered a promising secondary raw material for the synthesis of mullite-containing refractory materials. The presence of iron, calcium, and

titanium oxides, as well as other impurities, in its composition can influence the sintering and phase formation processes during high-temperature treatment.

Chalk consists primarily of calcium carbonate and serves as a source of calcium oxide upon thermal decomposition. During firing, the CaO formed can interact with the aluminosilicate matrix, influencing the kinetics of phase formation, sintering processes, and the formation of the material's microstructure.

The results obtained indicate that the chemical composition of the components under study is conducive to the formation of mullite ceramics during high-temperature sintering and allows for an assessment of the effect of fly ash and calcium-containing additives on the formation of high-temperature aluminosilicate phases.

### *3.2. Phase Composition of Raw Materials*

The diffractogram of the clay is characterized by the presence of intense quartz ($SiO_2$) reflections at 2θ = 20.8°, 26.6°, and 50.1°, as well as less pronounced peaks corresponding to clay minerals of the kaolinite and illite groups. The results obtained indicate the predominance of an aluminosilicate component, characteristic of the raw materials used in the production of ceramic and refractory materials (Figure 2).

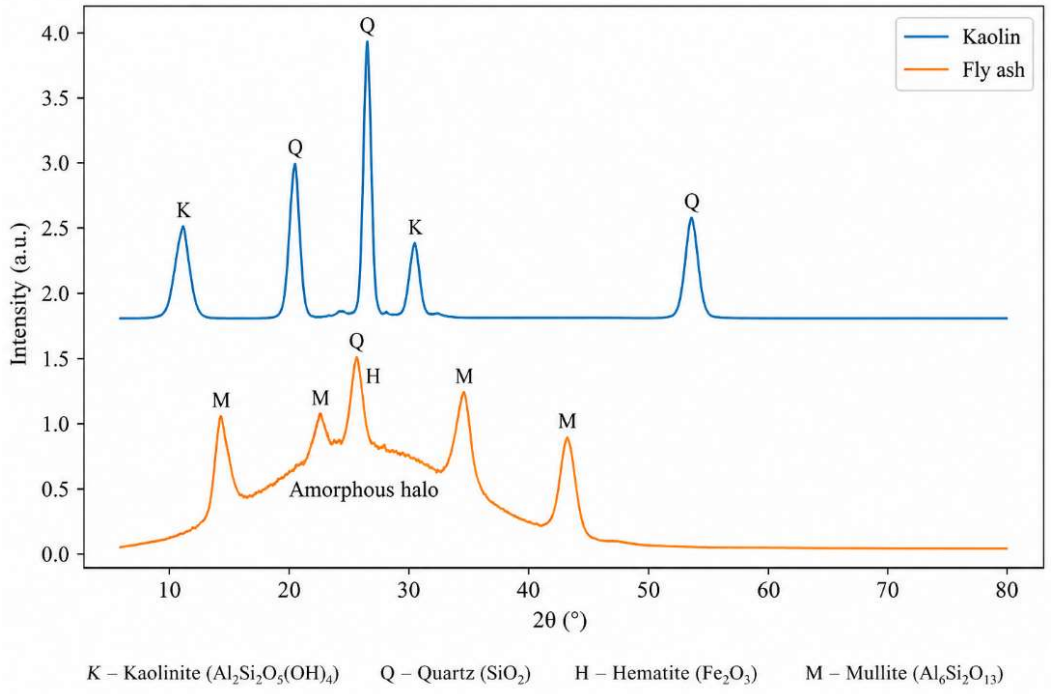



**Figure 2.** XRD patterns of clay and fly ash.

The XRD patterns of kaolin and fly ash demonstrate differences in their initial crystalline phase assemblages. The kaolin pattern is characterized primarily by reflections of kaolinite and quartz. Characteristic kaolinite reflections occur at approximately 2θ = 12.4° and 24.9°, while intense quartz reflections are observed near 20.8°, 26.6°, and 50.1°.

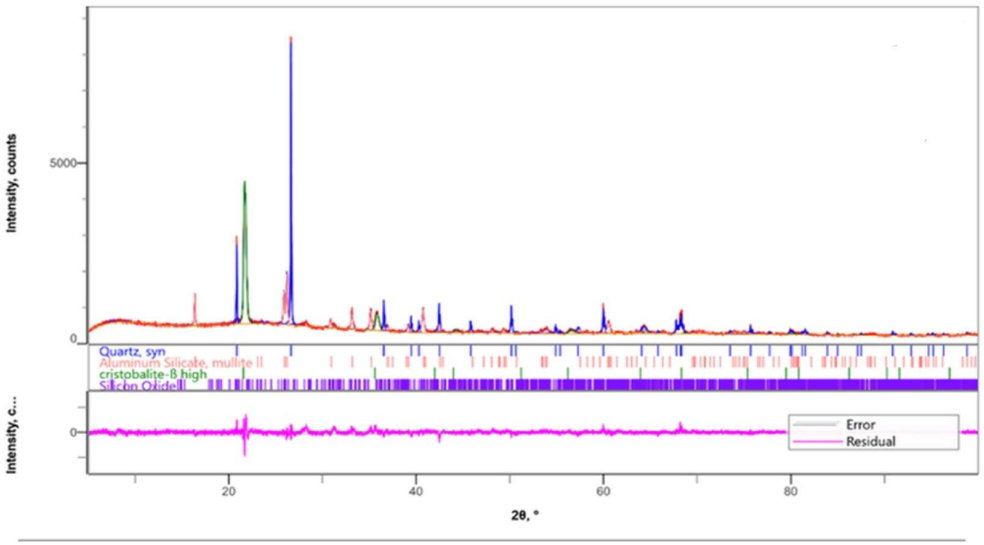
The fly-ash pattern contains crystalline quartz and mullite. The characteristic mullite reflections are observed at approximately 2θ = 16.4°, 26.0°, 33.2°, and 40.8°. In addition to the crystalline reflections, a broad diffuse halo in the region of approximately 18–35° is observed, which is attributed to the amorphous aluminosilicate component of the fly ash.

The coexistence of crystalline quartz and mullite with an amorphous aluminosilicate component indicates that fly ash can contribute both pre-existing crystalline phases and a reactive glassy component to the ceramic system. This feature is important for understanding the subsequent phase transformations during firing.

### *3.3. Quantitative Phase Composition of Fired Samples*

The XRD results demonstrate that the phase composition of the fired ceramics is influenced by both the initial composition and the firing temperature. Quantitative phase analysis was performed using the whole powder pattern fitting (WPPF) method based on the Fundamental Parameters approach. The results for the investigated compositions are presented in Figure 3.

(**a**)

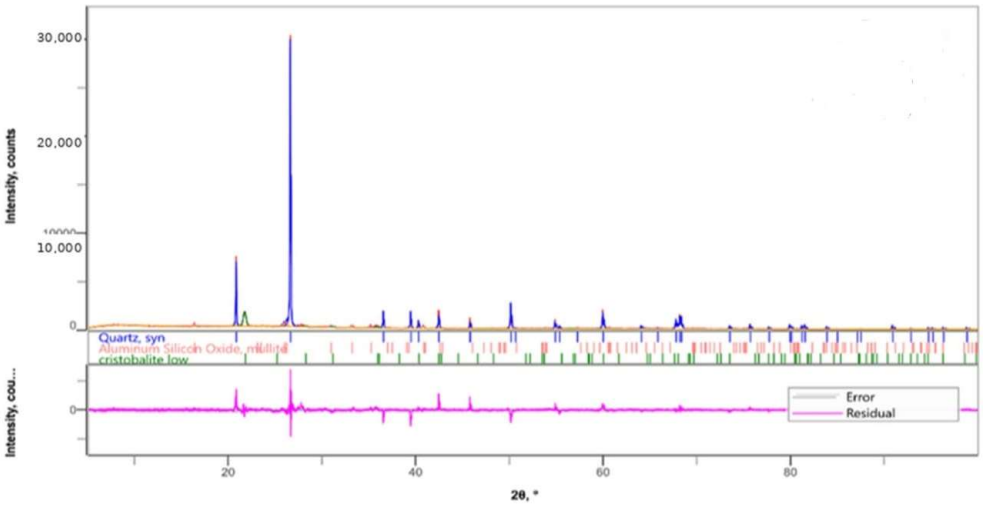



**WPPF legend**

Blue line: calculated pattern (WPPF fit)
Red line: observed pattern (experimental data)
Orange line: background
Colored vertical markers: Bragg reflection positions of the identified crystalline phases.

Quantitative phase composition (WPPF): Mullite — 42.0 wt%; Quartz ($SiO_2$) — 29.1 wt%; Cristobalite — 27.2 wt%; additional $SiO_2$ phase — 1.59 wt%.

(**b**)

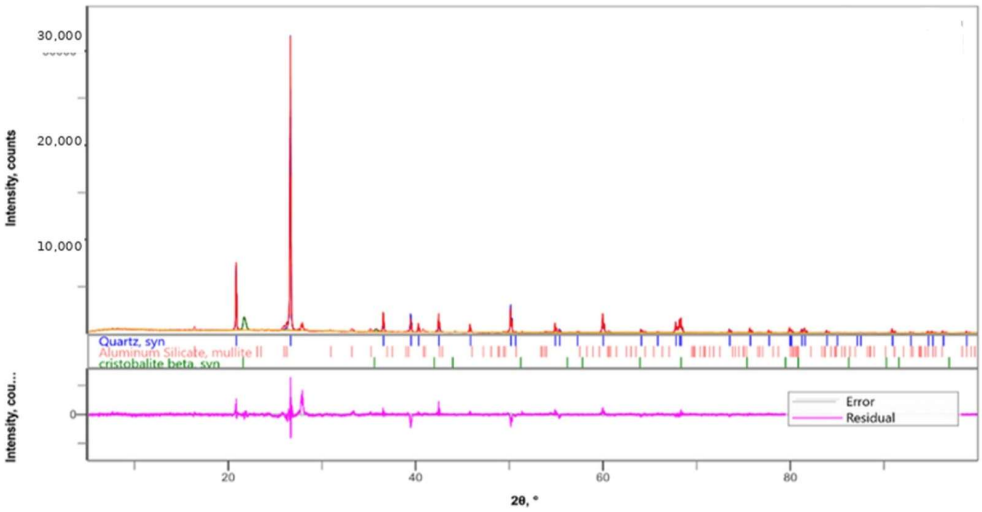



**WPPF legend**

Blue line: calculated pattern (WPPF fit)
Red line: observed pattern (experimental data)
Orange line: background
Colored vertical markers: Bragg reflection positions of the identified crystalline phases.

Quantitative phase composition (WPPF): Quartz ($SiO_2$) — 80.60 wt%; Mullite — 11.00 wt%; Cristobalite — 8.41 wt%.

(**c**)




**WPPF legend**

Blue line — calculated pattern (WPPF fit)

Red line — observed pattern (experimental data)

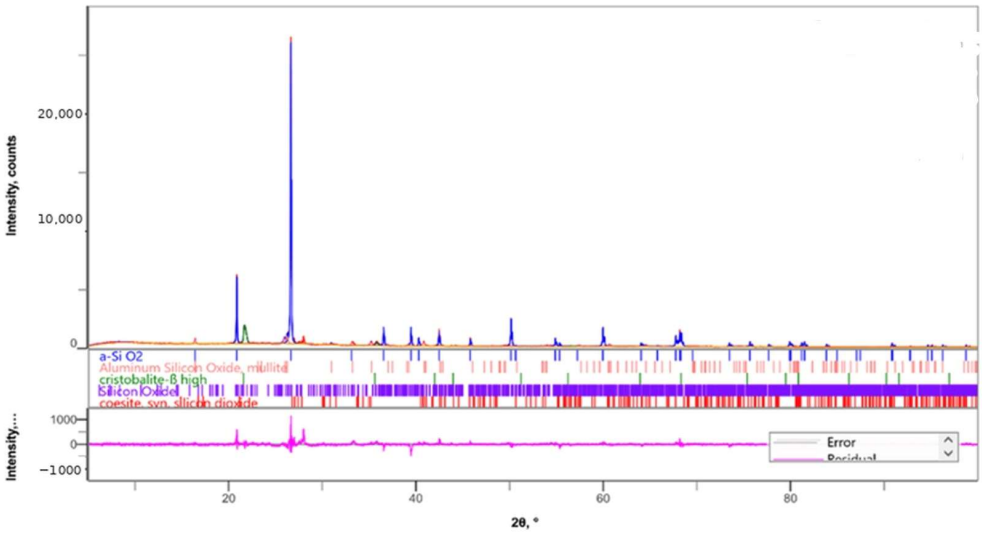
Orange line — background

Colored vertical markers — Bragg reflection positions of the identified crystalline phases

**Quantitative phase composition (WPPF)**

- Quartz ($SiO_2$) — 82.60 wt%
- Mullite — 10.70 wt%
- Cristobalite — 6.68 wt%

(**d**)




**WPPF legend**

Blue line: calculated pattern (WPPF fit)

Red line: observed pattern (experimental data)

Orange line: background

Colored vertical markers: Bragg reflection positions of the identified crystalline phases.

**Quantitative phase composition (WPPF):**

- α-$SiO_2$ (quartz) — 91.25 wt%
- Mullite — 4.93 wt%
- Cristobalite — 2.92 wt%
- Additional $SiO_2$ phase — 0.57 wt%
- Coesite — 0.32 wt%

(**e**)

**Figure 3.** Results of quantitative phase analysis of the KER-1, KER-2, and KER-3 samples after firing at 1300 and 1450 °C using the whole-pattern fitting (WPPF) method: (**a**) KER-1 at 1450 °C; (**b**) KER-1 at 1300 °C; (**c**) KER-2 at 1450 °C; (**d**) KER-2 at 1300 °C; and (**e**) KER-3 at 1300 °C.

The X-ray phase analysis demonstrates that both the chemical composition of the initial mixture and the firing temperature have a pronounced effect on the crystalline phase assemblage in the kaolin–fly ash–chalk system. The investigated compositions contained 30–60 wt% fly ash, with the remaining fraction consisting mainly of kaolin and 1 wt% chalk. The main crystalline phases identified in the fired ceramics were quartz ($SiO_2$), mullite, and cristobalite, indicating the occurrence of high-temperature phase transformations within the aluminosilicate system.

The highest relative proportion of mullite was observed in KER-1 fired at 1300 °C. According to the WPPF analysis, this sample contained 42.0 wt% mullite, 29.1 wt% quartz, and 27.2 wt% cristobalite, together with 1.59 wt% of an additional $SiO_2$ phase. The presence of mullite in the fired sample may partly reflect the retention of pre-existing mullite from the fly ash, while additional phase transformations may also occur during firing. The relatively high proportion of mullite among the quantified crystalline phases indicates its significant contribution to the crystalline phase assemblage at this temperature. The XRD results are consistent with the SEM observations, which show a continuous aluminosilicate matrix, although individual spherical fly ash particles and residual pores are still present.

For comparison, KER-1 fired at 1450 °C contained 73.7 wt% $\alpha$-$SiO_2$, 21.0 wt% mullite, and two cristobalite modifications with a combined content of approximately 5.25 wt%. Thus, increasing the firing temperature from 1300 to 1450 °C did not increase the relative proportion of mullite in KER-1. Instead, the relative proportion of quartz increased substantially, while that of mullite decreased. This result demonstrates that the effect of firing temperature on the relative crystalline phase composition is not necessarily monotonic and depends strongly on the initial formulation and the redistribution of crystalline phases during firing.

KER-2 exhibited a different phase relationship (Figure 3c,d). At 1300 °C, the sample contained predominantly quartz (82.6 wt%), while mullite accounted for 10.7 wt% and cristobalite for 6.68 wt%. After firing at 1450 °C, the phase composition remained dominated by quartz (80.6 wt%), with 11.0 wt% mullite and 8.41 wt% cristobalite. The increase in the relative proportion of mullite was therefore small, approximately 0.3 percentage points. This indicates that the change in the relative mullite proportion with increasing firing temperature was limited for this composition under the investigated conditions.

KER-3 fired at 1300 °C (Figure 3e) was also dominated by $\alpha$-$SiO_2$ (91.25 wt%), whereas the relative proportion of mullite was 4.93 wt%, accompanied by cristobalite (2.92 wt%) and additional $SiO_2$-related phases. The WPPF refinement also indicated minor amounts of $SiO_2$ (0.57 wt%) and a phase identified as coesite (0.32 wt%).

Overall, the XRD results indicate that the crystalline phase assemblage depends on the combined effects of the initial raw material composition and firing temperature. The detected mullite may partly originate from the pre-existing mullite phase in the fly ash, which remains present after high-temperature treatment, while additional phase transformations may also occur during firing. The highest relative proportion of mullite among the investigated compositions was observed in KER-1 fired at 1300 °C (42.0 wt%). These findings highlight the importance of selecting an appropriate initial mixture composition and firing regime for producing mullite-containing aluminosilicate ceramics.

It should be noted that the WPPF values represent normalized proportions of the crystalline phases included in the refinement and do not directly indicate the absolute phase contents in the bulk samples.

### *3.4. SEM Analysis of the Microstructure of Samples*

The SEM micrographs were used to qualitatively examine particle morphology, the arrangement of aggregates, interparticle contacts, and the presence and distribution of pores in the investigated samples. Particular attention was paid to microstructural differences associated with fly ash content and firing temperature.

The SEM observations were considered alongside the XRD results to discuss the relationship between the crystalline phase composition and the morphological features of the fired materials. It should be noted that SEM imaging was performed in secondary electron (SE) mode. Therefore, the micrographs provide information primarily on surface morphology and cannot independently establish the phase or elemental composition of individual microstructural regions. Phase identification and quantitative phase analysis were based on the XRD and WPPF results.

The control composition without fly ash is presented in Figure 4.

The KER-0 control composition exhibits a relatively developed pore structure, non-uniform grain distribution, and regions with limited particle consolidation. Pores and loosely connected particle aggregates remain visible even at higher firing temperatures. These morphological features indicate that the microstructure of the control composition remains relatively heterogeneous under the investigated firing conditions.

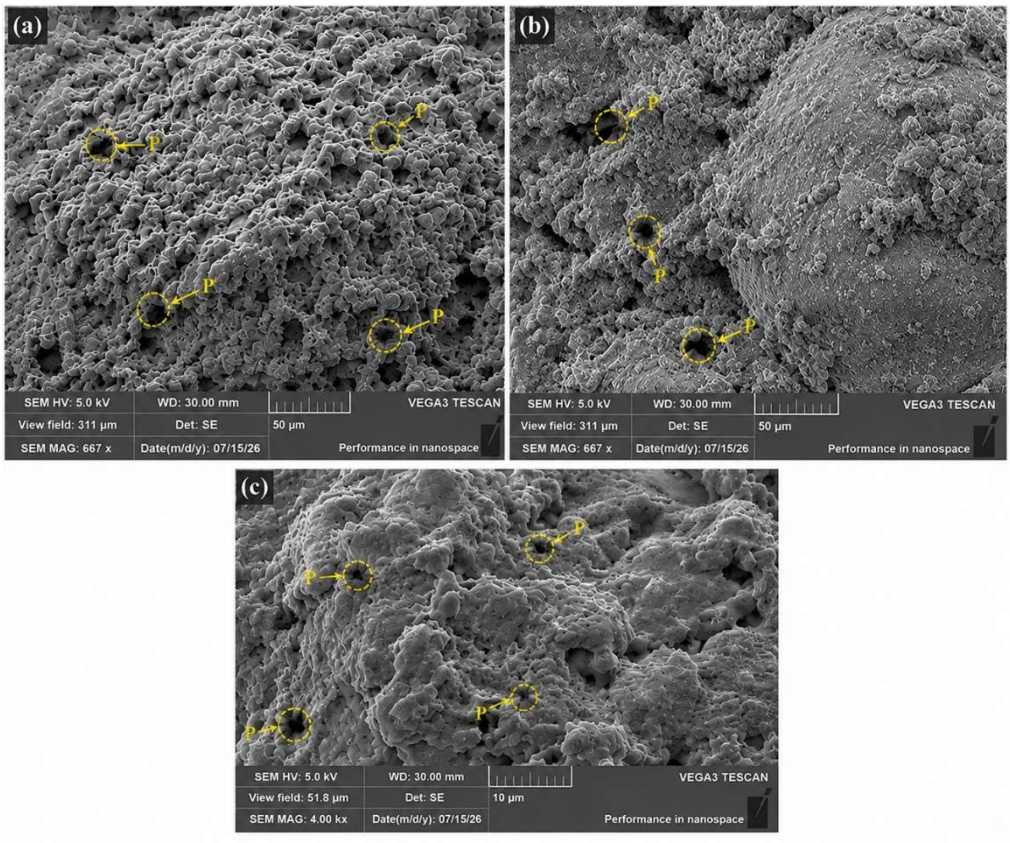



**Figure 4.** SEM micrographs of the KER-0 sample after firing at (**a**) 1200 °C, (**b**) 1300 °C, and (**c**) 1450 °C. Yellow dashed circles and arrows indicate residual pores (P). Magnifications: (**a**,**b**) 667×; (**c**) 4000×.

The KER-1 composition, containing 39% kaolin, 60% fly ash, and 1% chalk, exhibits noticeable changes in microstructure with increasing firing temperature (Figure 5).

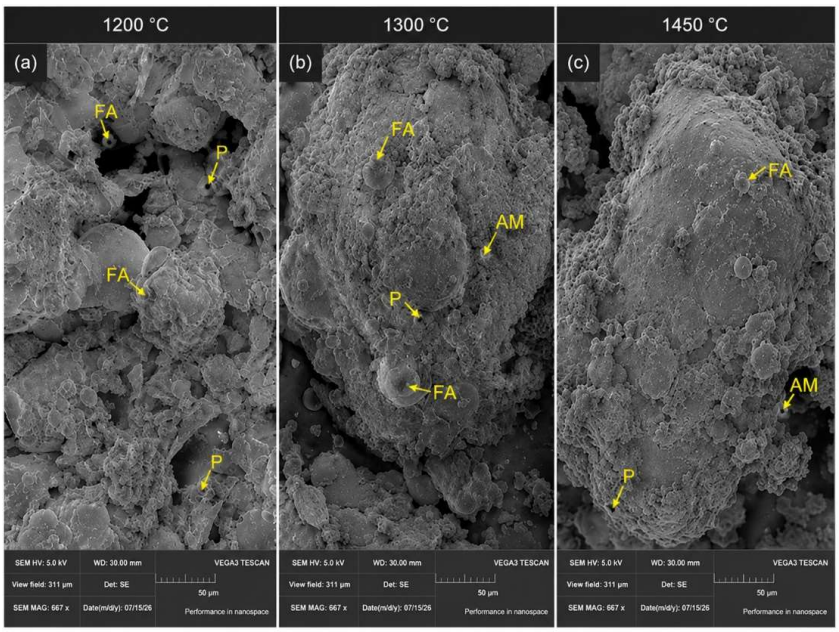



**Figure 5.** SEM micrographs of the KER-1 sample after firing at (**a**) 1200 °C, (**b**) 1300 °C, and (**c**) 1450 °C (magnification: 667×). FA—residual fly ash particle; P—residual pore; AM—aluminosilicate matrix.

At 1300 °C, a comparatively continuous aluminosilicate matrix is observed, incorporating partially consolidated aggregates. Individual spherical particles, attributed to the original fly ash morphology, and isolated pores are also visible. At 1450 °C, the microstructure appears more compact, with more pronounced contacts between adjacent particles and fewer visibly open pores. Some spherical particles retain their original morphology but appear partially incorporated into the surrounding matrix. These observations suggest an increase in the degree of microstructural consolidation at the higher firing temperature. However, this morphological change does not correspond to an increase in the relative mullite content determined by WPPF analysis.

For KER-2, the microstructure at 1300 °C is characterized by the presence of spherical particles, irregular aggregates, and visible pores (Figure 6).

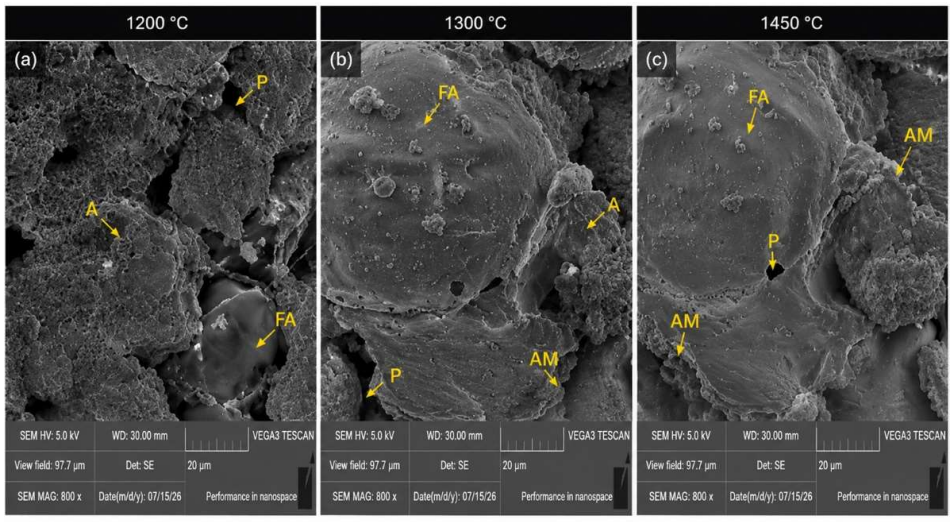



**Figure 6.** SEM micrographs of the KER-2 sample after firing at (**a**) 1200 °C, (**b**) 1300 °C, and (**c**) 1450 °C (magnification: 800×). FA—residual fly ash particle; A—aluminosilicate aggregate formed by the interaction between fly ash and kaolin; AM—aluminosilicate matrix; P—residual pore.

The contacts between individual structural elements appear less developed than those observed in the sample fired at 1450 °C. At the higher temperature, the microstructure appears more compact and homogeneous, with more pronounced interparticle contacts and partial incorporation of spherical particles into the surrounding matrix. These morphological differences suggest that increasing the firing temperature promotes microstructural consolidation. Nevertheless, the degree of microstructural consolidation should be distinguished from the relative mullite content, which is determined independently by XRD and WPPF analysis. The KER-3 micrographs show a comparatively compact surface with less distinct boundaries between some adjacent structural elements (Figure 7).

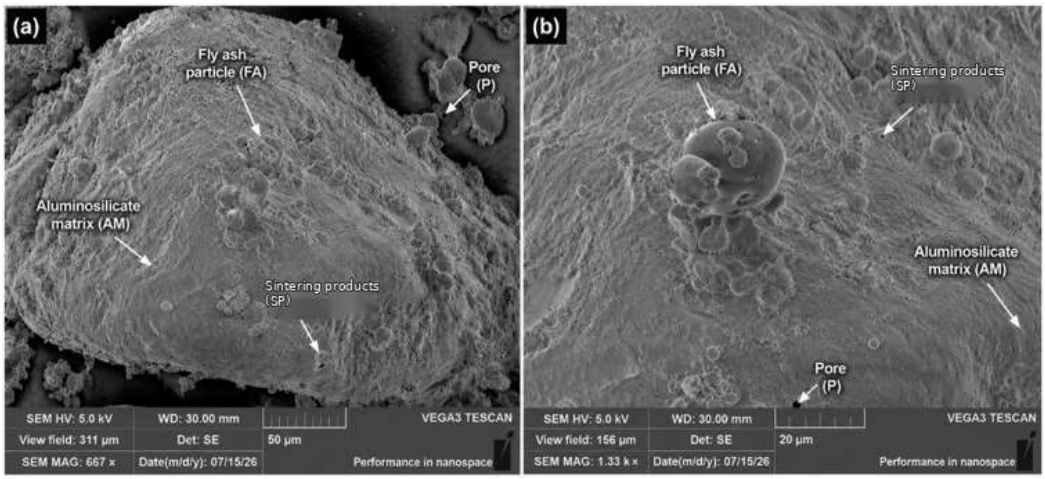



**Figure 7.** SEM micrographs of the KER-3 sample fired at 1450 °C: (**a**) 667× magnification; (**b**) 1330× magnification. FA—partially preserved spherical fly ash particle; AM—aluminosilicate matrix; SP—sintering products formed during high-temperature treatment; P—isolated residual pore.

Individual spherical particles retain recognizable morphological features, although some appear partially incorporated into the surrounding matrix. Fine surface features are also visible on certain particles. However, their chemical or phase identity cannot be established from SE images alone. Isolated pores remain visible in the examined regions.

Overall, the SEM observations reveal differences in particle morphology, aggregate arrangement, and the apparent degree of microstructural consolidation among the investigated compositions and firing conditions. The micrographs suggest that firing at higher temperatures is associated with a more compact appearance of the examined structures. These observations complement the XRD results but do not independently confirm the identity or quantity of crystalline phases. In particular, microstructural consolidation and quantitative mullite formation should be considered as distinct characteristics of the fired materials.

### *3.5. FTIR Analysis*

The FTIR spectra were analyzed with particular attention to the spectral regions associated with hydroxyl groups, carbonate groups, Si–O vibrations, and Si–O–Al structural units. Changes in the characteristic absorption bands were used to evaluate the dehydroxylation of the kaolinite component, the decomposition of carbonate-containing compounds, and the structural rearrangement of the aluminosilicate framework during firing.

The FTIR spectra of all five investigated samples are presented together in Figure 8 to facilitate direct comparison of their characteristic absorption bands, including variations in band intensity, width, and shape.

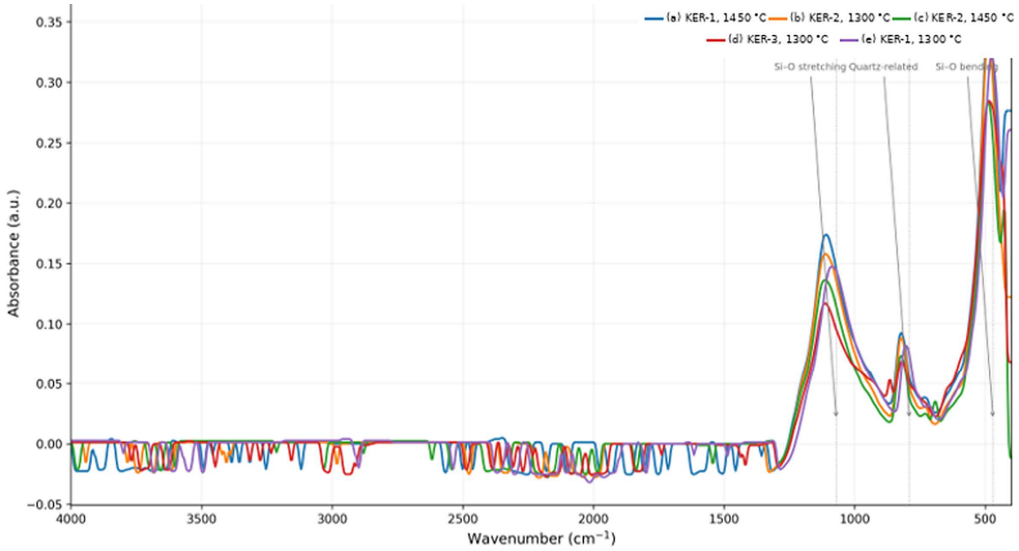



**Figure 8.** FTIR spectra of the fired ceramic samples: (**a**) KER-1 fired at 1450 °C; (**b**) KER-2 fired at 1300 °C; (**c**) KER-2 fired at 1450 °C; (**d**) KER-3 fired at 1300 °C; and (**e**) KER-1 fired at 1300 °C. The main absorption regions associated with Si–O stretching, quartz-related vibrations, and Si–O bending are indicated.

The most pronounced absorption feature occurs in the region of 1000–1100 $cm^{-1}$ and is mainly attributed to Si–O stretching vibrations in Si–O–Si and Si–O–Al structural units. This band represents the principal vibrational feature of the aluminosilicate network in the investigated samples. The absorption bands observed at approximately 450–500 $cm^{-1}$ are associated with Si–O bending vibrations. A weaker feature in the region of 780–800 $cm^{-1}$ is consistent with quartz-related vibrations. These assignments are in agreement with the characteristic FTIR features reported for fly ash–kaolin-based ceramic materials [16].

No clearly distinguishable absorption bands associated with structural OH groups are observed in the region of 3600–3700 $cm^{-1}$. This observation is consistent with the dehydroxylation of the kaolinite component during firing and the formation of thermally transformed aluminosilicate phases. In addition, the carbonate-related absorption regions at approximately 1400–1500, 870–880, and 710–730 $cm^{-1}$ exhibit very weak or poorly resolved features. This indicates substantial decomposition of carbonate-containing components during thermal treatment. However, the absence or low intensity of these bands does not by itself establish the complete absence of the corresponding compounds.

Comparison of the spectra obtained at 1300 and 1450 °C reveals no new dominant absorption bands. The main vibrational features remain in similar spectral regions, while differences in their relative intensity and shape indicate variations in the local bonding environment and structural organization of the fired materials. These changes are consistent with temperature-induced transformations of the aluminosilicate matrix.

Despite the variation in fly ash content from 30 to 60 wt%, the principal absorption bands remain within similar spectral regions. This suggests that the main types of aluminosilicate bonds are preserved across the investigated compositions. At the same time, differences in the crystalline phase proportions identified by X-ray diffraction are not necessarily reflected by substantial shifts in the FTIR band positions.

It should be noted that FTIR spectroscopy primarily characterizes chemical bonds and local structural units and is not sufficiently phase-selective for the quantitative determination of individual crystalline phases in these materials. Therefore, the identification and quantitative comparison of mullite, quartz, and cristobalite were based primarily on XRD analysis and whole-pattern fitting (WPPF), whereas FTIR was used as a complementary method to assess changes in the aluminosilicate bonding structure during firing.

Overall, the FTIR results provide complementary evidence of the preservation of the aluminosilicate bonding framework, dehydroxylation of kaolinite, and changes in the local structural environment during high-temperature firing. The characteristic absorption bands and their assignments are summarized in Table 4.

**Table 4.** Characteristic FTIR absorption bands of the fired ceramic samples.

| Wavenumber, $cm^{-1}$ | Assignment | Observed Change After Firing |
|---|---|---|
| 450–500 | Si–O deformation vibrations | Retained after firing |
| 780–800 | Vibrations associated with quartz | Consistent with residual quartz |
| 1000–1100 | Si–O–Si and Si–O–Al stretching vibrations | Dominant absorption band of the aluminosilicate network |
| 3600–3700 | OH stretching vibrations of kaolinite | No distinct absorption bands detected after firing |
| 1400–1500 | Carbonate ($CO_3^{2-}$) vibrations | Very weak or absent after firing |
| 870–880 | $CO_3^{2-}$ vibrations | Very weak or absent after firing |
| 710–730 | $CO_3^{2-}$ vibrations | Very weak or absent after firing |

The absence of distinct absorption bands in the 3600–3700 $cm^{-1}$ region, characteristic of structural OH groups in kaolinite, indicates that dehydroxylation of the initial kaolin occurred during firing. The characteristic carbonate-related bands at approximately 1400–1500, 870–880, and 710–730 $cm^{-1}$ were also very weak or absent, suggesting substantial decomposition of carbonate-containing components during firing. No additional distinct absorption bands appeared with increasing firing temperature from 1300 to 1450 °C.

## 4. Discussion

The results obtained confirm that fly ash from thermal power plants is a promising secondary aluminosilicate raw material for the production of refractory materials based on clay compositions. Its high content of silicon and aluminum oxides, together with the presence of an amorphous glass phase, may contribute to its participation in high-temperature phase transformations and sintering processes. The $Al_2O_3$–$SiO_2$–CaO phase diagram provides a basis for understanding the influence of the proportions of these oxides on the phase composition of aluminosilicate ceramics. The use of fly ash allows for the partial replacement of kaolin; however, the influence of its chemical and mineralogical composition on phase development and microstructural evolution requires further investigation.

In recent years, the use of industrial aluminosilicate waste has been viewed as one of the key areas of development for the refractory and ceramics industries. The limited reserves of high-quality natural raw materials, the rising cost of their extraction, and the need to implement the principles of the circular economy have led to the active use of fly ash, coal gangue, red mud, and other industrial wastes as alternative sources of aluminosilicates [32–34]. Among these materials, fly ash is of particular interest due to its combination of high $SiO_2$ and $Al_2O_3$ contents with an amorphous glass phase that may participate in solid-state and liquid-assisted reactions during heating.

According to the literature, the addition of fly ash not only allows for the partial replacement of expensive natural raw materials but may also influence sintering processes due to the presence of reactive aluminosilicate components. The relatively high proportion of mullite observed in the crystalline phase assemblage of KER-1 after firing at 1300 °C is consistent with previous studies showing that mullite formation from kaolin begins at approximately 1050–1100 °C and develops progressively with increasing temperature [35–37]. However, since mullite was already present in the initial fly ash used in this study, its detection after firing cannot be attributed exclusively to its formation through reactions between kaolin and fly ash. The effectiveness of using ash depends significantly on its origin, the contents of calcium, iron, and alkali metal oxides, as well as the amount and

characteristics of the residual glass phase, all of which may influence liquid-phase sintering and the final phase composition of the material [38].

The results of the present study can be considered in the context of previous investigations of fly ash-based mullite ceramics, although the processing approaches and research objectives differ. Luo et al. [34] demonstrated the feasibility of producing mullite-based ceramic tiles using high-alumina fly ash as the primary raw material. Koshy et al. [6] investigated the development of mullite structures from fly ash, while Valášková et al. [35] examined the influence of kaolin additions on the sintering behavior and properties of fly ash-based mullite ceramics. Chen et al. [36] focused on porous mullite ceramics fabricated from fly ash hollow spheres and kaolin, whereas Wan et al. [20] investigated the preparation of high-strength, low-thermal-conductivity mullite refractories based on fly ash reconstruction. In comparison with these studies, the present work focuses on the relationship between the initial oxide composition, the degree of kaolin substitution by fly ash, and firing temperature in a kaolin–fly ash–chalk system. The use of the $Al_2O_3$–$SiO_2$–CaO phase diagram for preliminary compositional selection, together with the combined XRD, WPPF, SEM, and FTIR analyses, provides complementary information on composition-dependent phase development and microstructural changes during firing.

The results obtained in this study are consistent with these general trends. X-ray phase analysis confirmed the presence of quartz, mullite, and cristobalite in the fired ceramics. The detected mullite may partly originate from the pre-existing mullite phase in the fly ash, which remained present after high-temperature treatment. At the same time, additional phase transformations within the aluminosilicate system may occur during firing. However, the available XRD data do not allow the quantitative contribution of newly formed mullite to be distinguished from that of the initial mullite. Therefore, the phase composition is discussed in terms of the relative proportions of the crystalline phases identified by WPPF rather than as direct evidence of mullite formation through the interaction of kaolin and fly ash.

The results of the microstructural analysis also revealed changes associated with increasing firing temperature. SEM observations showed differences in particle packing, intergranular contacts, and matrix morphology. The more compact appearance of the ceramic matrix at higher temperatures may be associated with particle rearrangement, sintering, and possible liquid-phase formation. Nevertheless, SEM observations provide qualitative information about local microstructural features and do not independently establish bulk densification, reduced open porosity, or improved refractory performance.

It should be noted that the effect of fly ash depends on its proportion in the composition and its specific chemical and mineralogical characteristics. The balance between aluminosilicate components and fluxing oxides may influence sintering kinetics, phase development, and the resulting microstructure. An excessive increase in ash content may alter the relative proportions of crystalline and amorphous phases and affect the structural characteristics of the fired material. This highlights the need to optimize the composition while taking into account the chemical and mineralogical characteristics of the specific ash.

One of the current trends in improving aluminosilicate refractories is the use of micro- and nano-modifying additives, primarily nano-$Al_2O_3$ and nano-$SiO_2$. Due to their high specific surface area, nanoparticles may accelerate solid-state interaction processes, influence the onset of sintering, promote structural development, and serve as nucleation sites for mullite crystals. This may make it possible to produce materials with a more uniform microstructure, increased mechanical strength, and improved thermal stability while reducing energy consumption [39–41]. Although nanoadditives were not used in this study, their combined use with fly ash represents a promising area for further research.

Overall, an analysis of the published works [42–45] indicates that the current development of aluminosilicate refractories is based on three interrelated areas: expanding the use of industrial waste as a secondary raw material, controlling phase development through optimization of chemical composition and heat treatment conditions, and modifying the structure using micro- and nano-additives.

The observed phase assemblage is consistent with previous studies of fly ash–kaolin systems, in which fly ash contributes both crystalline phases, such as quartz and mullite, and an amorphous aluminosilicate component that may participate in high-temperature reactions and sintering [46]. The presence of mullite in the fired compositions should therefore be considered in relation to both the mineralogical composition of the initial fly ash and the possible phase transformations occurring during heat treatment.

The decrease in the relative proportion of mullite observed for KER-1 with increasing firing temperature from 1300 to 1450 °C does not necessarily indicate a reduction in its absolute content in the bulk material. Since WPPF provides normalized proportions of the crystalline phases included in the refinement, the observed change may reflect variations in the relative distribution of crystalline phases, particularly the substantial increase in the quartz fraction. Previous studies have shown that increasing the firing temperature can promote mullite crystal growth and microstructural development in kaolin-based ceramics. Therefore, the lower relative mullite fraction determined by WPPF for KER-1 at 1450 °C should not be interpreted as direct evidence of mullite decomposition or suppression of its formation. SEM observations revealed a more compact-looking matrix and improved intergranular contacts at 1450 °C, indicating changes in the local microstructure during high-temperature treatment [47,48].

The practical significance of this work lies in the possibility of utilizing fly ash from thermal power plants in the production of refractory materials. This approach may contribute to reducing the consumption of natural aluminosilicate raw materials, decreasing the volume of industrial waste requiring disposal, and mitigating environmental impacts. These objectives are consistent with modern principles of resource conservation, the circular economy, and sustainable development.

Thus, the results of this study demonstrate the potential of using fly ash from thermal power plants as a secondary component in refractory materials based on clay raw materials. The findings provide further insight into the relationship between the initial chemical and mineralogical composition of raw materials, firing temperature, and the resulting crystalline phase assemblage in the $Al_2O_3$–$SiO_2$ system. They can serve as a basis for further optimization of compositions and processing conditions for the production of mullite-containing aluminosilicate ceramics.

## 5. Conclusions

The results demonstrated that the phase composition of the fired kaolin–fly ash–chalk ceramics was governed by the combined effects of the initial raw material composition and firing temperature. Fly ash content alone did not determine the relative proportion of mullite, indicating the importance of the overall aluminosilicate composition and the characteristics of the starting materials. The detected mullite may partly originate from the pre-existing mullite phase in the fly ash.

Among the investigated compositions and firing conditions, KER-1 fired at 1300 °C exhibited the highest relative proportion of mullite among the quantitatively analysed crystalline phases (42.02 wt%). Increasing the firing temperature to 1450 °C resulted in a decrease in the relative mullite proportion to 21.02 wt%, confirming that higher firing temperatures do not necessarily favor mullite enrichment in the investigated ceramic system.

SEM and FTIR analyses confirmed the formation of an aluminosilicate ceramic structure after firing. The samples fired at 1450 °C exhibited more pronounced microstructural

consolidation and interparticle contacts, while FTIR analysis confirmed the development of an aluminosilicate structural framework, dehydroxylation of kaolinite, and decomposition of carbonate-containing components.

Overall, KER-1 fired at 1300 °C demonstrated the most favorable phase composition in terms of the relative mullite proportion among the investigated conditions. These findings provide a basis for optimizing the composition and firing conditions of fly ash-based mullite-containing ceramic materials. Further investigations of mechanical strength, thermal properties, and high-temperature performance are required to establish their suitability for refractory applications.

**Author Contributions:** Conceptualization, L.S. and R.N.; methodology, R.N., T.A. and M.S.; software, L.S., D.S. and M.S.; validation, T.A. and M.B.; formal analysis, M.B.; investigation, L.S., R.N. and D.S.; resources, L.S., D.S. and M.S.; data curation, L.S., T.A. and M.B.; writing—original draft preparation, L.S.; writing—review and editing, L.S., R.N., M.S. and M.B.; visualization, T.A. and M.B.; supervision, R.N. and M.B.; project administration, R.N. All authors have read and agreed to the published version of the manuscript.

**Funding:** This research has been funded by the Science Committee of the Ministry of Science and Higher Education of the Republic of Kazakhstan (Grant No. AP26193815 Development of scientific and technical bases of refractory materials technology using wastes of power engineering enterprises).

**Data Availability Statement:** The original contributions presented in this study are included in the article. Further inquiries can be directed to the corresponding authors.

**Acknowledgments:** This research was carried out within the framework of scientific cooperation between AGH University of Kraków and Kazakh Agro-Technical Research University. The authors would like to thank the Faculty of Mechanical Engineering and Robotics at AGH University of Krakow for the organizational and technical support provided during this research. The research presented in this article will form part of the PhD thesis of Lazzat Shansharova, conducted under the supervision of Rimma Niyazbekova and Michał Bembenek.

**Conflicts of Interest:** The authors declare no conflicts of interest.

## References

1. Krasnyi, B.L.; Ikonnikov, K.I.; Lemeshev, D.O.; Sizova, A.S. Fly Ash as Technogenic Raw Material for Producing Refractory and Insulating Ceramic Materials (Review). *Glass Ceram.* **2021**, *78*, 48–56 https://doi.org/10.1007/s10717-021-00347-3.
2. Mathapati, M.; Amate, K.; Durga Prasad, C.; Jayavardhana, M.L.; Hemanth Raju, T. A review on fly ash utilization. *Mater. Today Proc.* **2022**, *50*, 1535–1540.
3. Nsiah-Gyambibi, R.; Sokama-Neuyam, Y.A.; Boakye, P.; Ampomah, W.; Aggrey, W.N.; Wang, S.; Zhang, S.; Wang, S. Valorization of coal fly ash (CFA): A multi-industry review. *Int. J. Environ. Sci. Technol.* **2023**, *20*, 12807–12822. https://doi.org/10.1007/s13762-023-04895-9.
4. Rumi, M.K.; Irmatova, S.K.; Fayziev, S.A.; Urazaeva, E.M.; Mansurova, E.P.; Zufarov, M.A. Production of the aluminosilicate ceramic materials using fly ash from thermal power plants (TPP). *Novye Ogneupory* **2020**, *5*, 37–40. (In Russian) https://doi.org/10.17073/1683-4518-2020-5-37-40.
5. Hossain, S.S.; Roy, P. Sustainable ceramics derived from solid wastes: A review. *J. Asian Ceram. Soc.* **2020**, *8*, 984–1009. https://doi.org/10.1080/21870764.2020.1815348.
6. Koshy, P.; Ho, N.; Zhong, V.; Schreck, L.; Koszo, S.; Severin, E.; Sorrell, S. Fly Ash Utilisation in Mullite Fabrication: Development of Novel Percolated Mullite. *Minerals* **2021**, *11*, 84. https://doi.org/10.3390/min11010084.
7. Valášková, M.; Blahůšková, V.; Edelmannová, M.F.; Matějová, L.; Soukup, K.; Plevová, E. Clay/Fly Ash Bricks Evaluated in Terms of Kaolin and Vermiculite Precursors of Mullite and Forsterite, and Photocatalytic Decomposition of the Methanol–Water Mixture. *Minerals* **2023**, *13*, 1114. https://doi.org/10.3390/min13091114.

8. Sánchez-Soto, P.J.; Eliche-Quesada, D.; Martínez-Martínez, S.; Pérez-Villarejo, L.; Garzón, E. Study of a Waste Kaolin as Raw Material for Mullite Ceramics and Mullite Refractories by Reaction Sintering. *Materials* **2022**, *15*, 583. https://doi.org/10.3390/ma15020583.
9. Zierold, K.M.; Odoh, C. A review on fly ash from coal-fired power plants: Chemical composition, regulations, and health evidence. *Rev. Environ. Health* **2020**, *35*, 401–418.
10. Zhao, P.; Ma, S.; Wang, X.; Zhang, Y. Multiscale Structural Characterization and Regulatory Mechanisms of Fly Ash for Mullite Ceramic Applications. *Mater. Res. Bull.* **2026**, *196*, 113924. https://doi.org/10.1016/j.materresbull.2025.113924.
11. de Brito, I.P.; de Almeida, E.P.; de Araújo Neves, G.; de Lucena Lira, H.; Menezes, R.R.; da Silva, V.J.; de Lima Santana, L.N. Development of cordierite/mullite composites using industrial wastes. *Int. J. Appl. Ceram. Technol.* **2021**, *18*, 253–261. https://doi.org/10.1111/ijac.13622.
12. Sun, Z.; Zheng, Q.; Ma, C.; Wang, Y.; Cai, B.; Zheng, Y.; Wang, X.; Li, Y. Sintering Properties and Phase Evolution of Coal-Series Kaolin. *Ceram. Int.* **2026**, *52*, 57857–57867. https://doi.org/10.1016/j.ceramint.2026.09.382.
13. López-Perales, J.F.; Díaz-Tato, L.; Costilla-Aguilar, S.U.; González-Carranza, Y.; de Contreras León, J.E.; Rodríguez-Castellanos, E.A. Fly Ash as a Secondary Raw Material Improving the Sustainable Characteristics of a Conventional Silicoaluminate Refractory Castable. *Inorganics* **2025**, *13*, 367. https://doi.org/10.3390/inorganics13110367.
14. Du, Y.; Chen, M.; Wang, K.; Wang, T.; Wang, L. Integrating Fly Ash into High-Temperature Ceramic Glazes. *Sustainability* **2025**, *17*, 8017. https://doi.org/10.3390/su17178017.
15. Romero, M.; Padilla, I.; Contreras, M.; López-Delgado, A. Mullite-Based Ceramics from Mining Waste: A Review. *Minerals* **2021**, *11*, 332. https://doi.org/10.3390/min11030332.
16. Ritz, M. Infrared and Raman Spectroscopy of Mullite Ceramics Synthesized from Fly Ash and Kaolin. *Minerals* **2023**, *13*, 864. https://doi.org/10.3390/min13070864.
17. Plevová, E.; Vaculíková, L. Thermal Behavior of Ceramic Bodies Based on Fly Ash and Clay Minerals. *Minerals* **2024**, *14*, 334. https://doi.org/10.3390/min14040334.
18. Kotova, O.B.; Ustyugov, V.A.; Sun, S.; Ponaryadov, A.V. Mullite production: Phase transformations of kaolinite, thermodynamics of the process. *J. Min. Inst.* **2022**, *254*, 129–135. https://doi.org/10.31897/PMI.2022.43.
19. Tkach, E.V.; Nurbaturov, K.A. Investigation of the Chemical and Technological Principles for the Production of Aluminosilicate Refractories Based on Fly Ash. *Novye Ogneupory* **2021**, *1*, 45–50. https://doi.org/10.17073/1683-4518-2021-1-45-50. (In Russian)
20. Wan, X.; Sang, S.; Ma, Y.; Zhu, T. Preparation of high strength and low thermal conductivity mullite refractories based on reconstruction of fly ash. *Int. J. Appl. Ceram. Technology*. **2022**, *19*, 2749–2760. https://doi.org/10.1111/ijac.14098.
21. Wang, C.; Xu, G.; Gu, X.; Gao, Y.; Zhao, P. High value-added applications of coal fly ash in the form of porous materials: A review. *Ceram. Int.* **2021**, *47*, 22302–22315. https://doi.org/10.1016/j.ceramint.2021.05.070.
22. Bareiro, W.G.; De Andrade Silva, F.; Sotelino, E.D.; Gomes, O.D.F.M. The influence of alumina content on the chemical and mechanical behavior of refractory concretes fired at different temperatures. *Constr. Build. Mater.* **2018**, *187*, 1214–1223. https://doi.org/10.1016/j.conbuildmat.2018.08.065.
23. Fu, L.; Gu, H.; Huang, A.; Or, S.W.; Zou, Y.; Zou, Y.; Zhang, M. Design, fabrication and properties of lightweight wear lining refractories: A review. *J. Eur. Ceram. Soc.* **2022**, *42*, 744–763. https://doi.org/10.1016/j.jeurceramsoc.2021.11.019.
24. Antonovič, V.; Stonys, R.; Boris, R.; Malaiskiene, J. Effect of quartz sand on the properties and alkali resistance of refractory aluminosilicate castables. *Constr. Build. Mater.* **2022**, *351*, 128978. https://doi.org/10.1016/j.conbuildmat.2022.128978.
25. Díaz-Tato, L.; López-Perales, J.F.; González-Carranza, Y.; de Contreras León, J.E.; Rodríguez-Castellanos, E.A. Physico-Mechanical Properties of an Aluminosilicate Refractory Castable Obtained After Chamotte Waste Recycling by Firing Method. *Waste* **2025**, *3*, 35. https://doi.org/10.3390/waste3040035.
26. Guillemin, F.; Duttine, M.; Lecomte-Nana, G.; El Hafiane, Y.; Peyratout, C.; Smith, A. Investigation of Iron Oxide and Kaolinite Interactions during Sintering under Controlled Atmosphere. *Appl. Clay Sci.* **2025**, *276*, 107945. https://doi.org/10.1016/j.clay.2025.107945.
27. Abdul, W. Thermodynamic Modelling of Portland Cement Clinker Production. Ph.D. Thesis, University of Aberdeen, Aberdeen, UK, 2023. Available online: https://www.marcusbannerman.co.uk/wahab_abdul_thesis.pdf (accessed on 18 November 2026) .
28. Eriksson, G.; Pelton, A.D. Critical Evaluation and Optimization of the Thermodynamic Properties and Phase Diagrams of the CaO–$Al_2O_3$, $Al_2O_3$–$SiO_2$, and CaO–$Al_2O_3$–$SiO_2$ Systems. *Metall. Trans. B* **1993**, *24*, 807–816. https://doi.org/10.1007/BF02663141.
29. Haccuria, E.; Crivits, T.; Hayes, P.C.; Jak, E. Selected Phase Equilibria Studies in the $Al_2O_3$–CaO–$SiO_2$ System. *J. Am. Ceram. Soc.* **2016**, *99*, 691–704. https://doi.org/10.1111/jace.13991.

30. Mao, H.; Hillert, M.; Selleby, M.; Sundman, B. Thermodynamic Assessment of the CaO–$Al_2O_3$–$SiO_2$ System. *J. Am. Ceram. Soc.* **2006**, *89*, 298–308. https://doi.org/10.1111/j.1551-2916.2005.00698.x.
31. Suleimenov, S.T.; Abduvaliev, T.A.; Verner, V.F. *Osnovy Fizicheskoi Khimii Silikatov i Tugoplavkikh Soedinenii [Fundamentals of Physical Chemistry of Silicates and Refractory Compounds]*; Mektep: Alma-Ata, Kazakhstan, 1989; p. 200.
32. Kurovics, E.; Ibrahim, J.F.M.; Tihtih, M.; Udvardi, B.; Nuilek, K.; Gömze, L.A. Examination of mullite ceramic specimens made by conventional casting method from kaolin and sawdust. *J. Phys. Conf. Ser.* **2020**, *1527*, 012034. https://doi.org/10.1088/1742-6596/1527/1/012034.
33. Tang, Y.; Shi, Y.; Li, Y.; Yuan, X.; Mu, R.; Wang, Q.; Ma, Q.; Hong, J.; Cao, S.; Zuo, J.; et al. Environmental and economic impact assessment of the alumina–carbon refractory production in China. *Clean Technol. Environ. Policy* **2019**, *21*, 1723–1737 https://doi.org/10.1007/s10098-019-01741-w.
34. Luo, Y.; Ma, S.; Zheng, S.; Liu, C.; Han, D.; Wang, X. Mullite-based ceramic tiles produced solely from high-alumina fly ash: Preparation and sintering mechanism. *J. Alloys Compd.* **2018**, *732*, 828–837. https://doi.org/10.1016/j.jallcom.2017.09.179.
35. Valášková, M.; Blahůšková, V.; Vlček, J. Effects of Kaolin Additives in Fly Ash on Sintering and Properties of Mullite Ceramics. *Minerals* **2021**, *11*, 887. https://doi.org/10.3390/min11080887.
36. Chen, S.; Cai, W.-H.; Wu, J.-M.; Ma, Y.-X.; Li, C.-H.; Shi, Y.-S.; Yan, C.-Z.; Wang, Y.-J.; Zhang, H.-X. Porous mullite ceramics with a fully closed-cell structure fabricated by direct coagulation casting using fly ash hollow spheres/kaolin suspension. *Ceram. Int.* **2020**, *46*, 17508–17513. https://doi.org/10.1016/j.ceramint.2020.04.046.
37. Akhtar, M.N.; Bani-Hani, K.A.; Akhtar, J.N.; Khan, R.A.; Nejem, J.K.; Zaidi, K. Flyash-based bricks: An environmental savior—A critical review. *J. Mater. Cycles Waste Manag.* **2022**, *24*, 1663–1678.
38. Ermagambet, B.T.; Kazakov, K.M.; Nurgaliyev, N.U. Method for Processing Ash and Slag Waste by Electric Discharge. Kazakhstan Patent No. 34099, IPC C10J 3/00; Application No. 2018/0719.1, 17 January 2020. (In Russian)
39. Lima, L.; Silva, K.; Menezes, R.; Santana, L.; Lira, H. Microstructural characteristics, properties, synthesis and applications of mullite: A review. *Cerâmica* **2022**, *68*, 126–142. https://doi.org/10.1590/0366-69132022683853184.
40. Watts, R.D.; Watts, C.D. Bricks and Method of Forming Bricks with High Coal Ash Content Using a Press Mold Machine and Variable Firing Trays. U.S. Patent US 9,776,921 B2, IPC C04B 33/00; C04B 33/132; C04B 33/32; Application No. 15/453,522, 3 October 2017. Available online: https://patents.google.com/patent/US9776921B2 (accessed on 18 July 2026).
41. Xia, B.; Wang, Z.; Gou, L.; Zhang, M.; Guo, M. Porous mullite ceramics with enhanced compressive strength from fly ash-based ceramic microspheres: Facile synthesis, structure, and performance. *Ceram. Int.* **2022**, *48*, 10472–10479. https://doi.org/10.1016/j.ceramint.2021.12.256.
42. Škamat, J.; Boris, R.; Malaiškienė, J.; Antonovič, V.; Stonys, R.; Kudžma, A. Possibilities to Recycle Thermal Power Plant By-Products in Refractory Castables. *Sustainability* **2024**, *16*, 6349. https://doi.org/10.3390/su16156349.
43. Stonys, R.; Malaiškienė, J.; Škamat, J.; Antonovič, V. Effect of hollow corundum microspheres additive on physical and mechanical properties and thermal shock resistance behavior of bauxite based refractory castable. *Materials* **2021**, *14*, 4736. https://doi.org/10.3390/ma14164736.
44. Yang, Z.; Yang, F.; Zhao, S.; Li, K.; Chen, Z.; Fei, Z.; Chen, Z. In-situ growth of mullite whiskers and their effect on the microstructure and properties of porous mullite ceramics with an open/closed pore structure. *J. Eur. Ceram. Soc.* **2021**, *41*, 299–308. https://doi.org/10.1016/j.jeurceramsoc.2021.09.045.
45. Fomenko, E.V.; Rogovenko, E.S.; Anshits, N.N.; Solovyov, L.A.; Anshits, A.G. Characterization of Silicate Glass/Mullite Composites Based on Coal Fly Ash Cenospheres as Effective Gas Separation Membranes. *Materials* **2023**, *16*, 6913. https://doi.org/10.3390/ma16216913.
46. Chen, C.Y.; Lan, G.S.; Tuan, W.H. Microstructural evolution of mullite during the sintering of kaolin powder compacts. *Ceram. Int.* **2000**, *26*, 715–720. https://doi.org/10.1016/S0272-8842(00)00009-2.
47. Shoval, S.; Boudeulle, M.; Panczer, G. Identification of the thermal phases in firing of kaolinite to mullite by using micro-Raman spectroscopy and curve-fitting. *Opt. Mater.* **2011**, *34*, 404–409. https://doi.org/10.1016/j.optmat.2011.08.031.
48. Garcia-Valles, M.; Cuevas, D.; Alfonso, P.; Martinez, S. Thermal behaviour of ceramics obtained from the kaolinitic clays of Terra Alta, Catalonia, Spain. *J. Therm. Anal. Calorim.* **2022**, *147*, 5303–5312. https://doi.org/10.1007/s10973-021-11075-9.


**Disclaimer/Publisher's Note:** The statements, opinions and data contained in all publications are solely those of the individual author(s) and contributor(s) and not of MDPI and/or the editor(s). MDPI and/or the editor(s) disclaim responsibility for any injury to people or property resulting from any ideas, methods, instructions or products referred to in the content.